Polarizable-bond model for second-harmonic generation

Bernardo S. Mendoza
Centro de Investigaciones en Optica, A.C. Apartado Postal 1-948, 37 000 León, GTO, Mexico

W. Luis Mochán
Laboratorio de Cuernavaca, Instituto de Física, Universidad Nacional Autónoma de Mexico, Apartado Postal 48-3, 62 251 Cuernavaca, Morelos, Mexico

(Received 18 April 1996)

We develop a theory for the calculation of the optical second-harmonic generation spectra of Si incorporating the nonlinear surface local field effect. Our model consists of four interpenetrated fcc lattices of nonlinearly polarizable bonds. Each of them is anisotropic and although they are centrosymmetric, they respond quadratically to the spatial inhomogeneities of the polarizing local field. The large gradient of the field induced at a bond due to the dipole moment of a neighbor leads to a second order polarization. In the bulk, each bond lies within a centrosymmetric environment, so this contribution is canceled out after summing over all other bonds. However, at the surface it is not compensated and it leads to a large nonlinear macroscopic response. Our model parameters are fitted to the nonlinear anisotropy measured at 1.17 and 2.34 eV. We calculate a linear anisotropy spectra for the (110) surface in agreement with previous measurements. Our nonlinear spectra show peaks at 1.65 eV for a strained (001) surface and at 1.75 eV for a (111) surface, in agreement with some recent experimental results. [S0163-1829(97)08104-6]

I. INTRODUCTION

The electric-dipolar quadratic susceptibility is a third rank tensor, and therefore it must be null within the bulk of any centrosymmetric system. For this reason, a large portion of the light with frequency 2ω reflected from an interface illuminated with monochromatic radiation at ω is surface originated, making second-harmonic generation (SHG) a sensitive optical surface probe for this class of systems. Besides being nondestructive and noninvasive, SHG has the added advantage of accessing surfaces such as buried interfaces, out of ultrahigh vacuum conditions and within arbitrary transparent ambients. However, the efficiency of the surface SHG is extremely low, of the order of[1] $1/c(a_B^3/\lambda e)^3 \approx 10^{-20}$ cm^2/W, where a_B is the Bohr radius, λ the wavelength, e the electronic charge, and c the speed of light, and very powerful laser systems are required for its observation. Most experiments have been performed only at a few selected frequencies, emphasizing the polar and azimuthal angular dependence of the signal for different crystal surfaces and combinations of incoming and outgoing polarizations.[2–12] The possible angular dependence of SHG is well understood from a phenomenological point of view, in terms of the independent components of the bulk and surface nonlinear susceptibilities and their symmetry originated constraints.[13–16]

The recent development of high power tunable lasers with a wide spectral range has stimulated experiments in nonlinear surface *spectroscopy*. In particular, SHG spectra have recently been measured for different clean, oxidized, and adsorbate covered surfaces of Si.[17,18] These spectra show a well developed peak close to $2\omega = 3.3$ eV. Its position and its relative insensitivity to surface conditions suggest that it is originated from a bulk transition between the valence and conduction bands, which becomes SH electric-dipolarly active close to the surface. More recently, nonlinear anisotropy and electroreflectance spectroscopy experiments have shown that different components of the nonlinear susceptibility peak at slightly different frequencies.[19–21] These peaks have been associated to particular interband bulk transitions frequency-shifted at the surface.

There are different theoretical approaches in the literature to calculate SHG. The nonlinear surface response of simple metals was estimated[22,23] and later calculated[24,25] within the hydrodynamic model, and microscopic calculations for simple metals have been performed using self-consistent jellium models.[26–28] A peak in the SHG spectrum has been predicted at the subharmonic of the ionization threshold[28] and giant resonances were obtained at the frequencies of the multipolar surface plasmon and its subharmonic.[29] The anisotropy due to lattice effects has been incorporated using a Boltzmann equation approach for systems with a nearly spherical Fermi surface[30] and within the ''Swiss cheese'' model[31] for noble metals.[32] On the other side, there are a few calculations of the SHG spectra of semiconductors. Simple analytical expressions for model semiconductors made up of a continuous distribution of polarizable entities[1] were obtained by neglecting crystallinity effects. The latter were incorporated[33–35] within a dipolium model that also accounts for local field effects. A more microscopic approach has been employed to calculate SHG from As terminated Si(111) slabs using a tight binding formalism.[36]

The purpose of the present paper is the development of a simple quantitative theory for the SHG spectra of semiconductor surfaces accounting in an approximate way for the bulk transitions and the crystalline symmetry. A previous successful theory for the surface *linear* response of natural Si incorporated the geometrical arrangement of the atoms at the surface through the surface local field effect.[37] In this paper we extend that theory to the nonlinear response. We expect

the local field effect to have large consequences in SHG through the following mechanism: Consider a localized polarizable entity and a semi-infinite crystal made up of its replicas. If each entity is centrosymmetric it would have no electric-dipole-allowed SH transition, though it may have electric-quadrupolar and magnetic-dipolar contributions proportional to $\vec{\mathcal{E}}_i \nabla \vec{\mathcal{E}}_i$, where $\vec{\mathcal{E}}_i$ is the local field acting at site i. The external field has a very slow spatial variation whose scale is of the order of the wavelength λ, although the field induced by a nearby entity j may have a very large variation, with a scale determined by the distance from j to i, r_{ij}, which of course is of atomic dimensions a. Different neighbors contribute to the gradient $\nabla \vec{\mathcal{E}}_i$ along different directions, so that, if the *site i* is itself centrosymmetric, these large gradients will cancel out among themselves, leaving only a small residual gradient of order $\mathcal{E}/\lambda$. This cancellation is no longer possible at the surface, where $|\nabla \vec{\mathcal{E}}| \approx \mathcal{E}/a$, yielding a large SH surface polarization. When written in terms of the macroscopic field $\vec{E}$ this surface polarization is then proportional to $\vec{E}\vec{E}/a$, which corresponds to a large surface allowed dipolar SH process. In this paper we develop the model above into a full calculation for Si surfaces, building upon a previous paper by Schaich and Mendoza.[33] Following Ref. 38, we take as our polarizable entities the interatomic bonds with appropriately defined linear and nonlinear polarizabilities. Thus, our model Si crystal consists of four interpenetrated semi-infinite fcc lattices. However, unlike Ref. 38, in our model we allow the centrosymmetric Si-Si bonds to respond nonlinearly to the *inhomogeneous* polarizing local field. Thus, we obtain a finite quadratic response due to the noncentrosymmetric *environment* at the surface; our SHG mechanism is additional to any other surface nonlinearity such as those that would arise due to the actual breakage of the centrosymmetry of the bonds themselves.[38] A short account of this model and its first results have been recently published.[39]

This paper is organized as follows. In Sec. II we obtain expressions for the nonlinear dipolar and quadrupolar microscopic polarizabilities of each (anisotropic) bond in terms of its linear polarizabilities along and across its axis. These expressions are exact for anisotropic harmonic oscillators. In Sec. III we relate the surface and bulk macroscopic susceptibilities to the bonds polarizabilities. In Sec. IV we present calculations for the anisotropy of the linear and nonlinear reflectance of different Si surfaces and their calculated SHG spectra, and we compare our results to the available experimental data. Finally, in Sec. V we discuss our conclusions.

II. MICROSCOPIC MULTIPOLAR SUSCEPTIBILITIES

A. A single bond

We consider first an anisotropic pointlike harmonic oscillator of cylindrical symmetry, with charge $e<0$ and mass m situated at the origin. For the time being, we choose x to be along the symmetry axis and y,z perpendicular to it, and we denote the resonant frequency that corresponds to the response parallel to the bond by $\omega_x = \omega_\parallel$, whereas the resonant frequency that corresponds to the perpendicular response is denoted by $\omega_y = \omega_z = \omega_\perp$.

We describe the quantum mechanical approach used to find the dynamical response of the oscillator to an external perturbation. This response is the one required to study SHG. We start with the unperturbed Hamiltonian

$$h = \sum_i \hbar \omega_i \left(a_i^\dagger a_i + \frac{1}{2} \right), \tag{1}$$

where $a_i^\dagger$ (a_i) are the creation (annihilation) operators whose basic commutators are

$$[a_i, a_j^\dagger] = \delta_{ij} \tag{2}$$

with $i,j = x$, y, or z. The position and momentum operator are given by

$$x_i = r_i (a_i + a_i^\dagger) \tag{3}$$

and

$$p_i = i m \omega_i r_i (a_i^\dagger - a_i), \tag{4}$$

with $r_i = \sqrt{\hbar/2m\omega_i}$. Now, we assume a time dependent monochromatic perturbing Hamiltonian h', i.e.,

$$h' = H'(e^{-i\omega t} + e^{i\omega t}), \tag{5}$$

with the perturbation given not only by the usual electric dipolar coupling, but also by the magnetic dipolar and electric quadrupolar interaction

$$H' = -\vec{p}\cdot\vec{\mathcal{E}} - \vec{m}\cdot\vec{\mathcal{B}} - \frac{1}{2}\overleftrightarrow{Q}:(\nabla\vec{\mathcal{E}}), \tag{6}$$

where $\vec{\mathcal{E}}$ is the *linear* local electric field amplitude at the origin, $\nabla\vec{\mathcal{E}}$ its gradient, and $\vec{\mathcal{B}}$ is the *linear* local magnetic field, $\vec{p} = e\vec{x}$ and $\overleftrightarrow{Q} = e\vec{x}\vec{x}$ are the electric dipole and quadrupole moment operators, while $\vec{m} = e\vec{x}\times\vec{p}/(2mc)$ is the magnetic dipole moment operator.

In order to calculate the induced change in the expectation value of an observable O, we use the Kubo formulas[40]

$$\langle \delta O^{(1)}(\omega) \rangle = \frac{1}{i\hbar} \int_0^\infty d\tau e^{i\omega\tau} \langle [O, H'(-\tau)] \rangle \tag{7}$$

and

$$\langle \delta O^{(2)}(2\omega) \rangle = \left(\frac{1}{i\hbar} \right)^2 \int_0^\infty d\tau_1 e^{i\omega\tau_1} \int_{\tau_1}^\infty d\tau_2 e^{i\omega\tau_2} \times \langle [[O, H'(-\tau_1)], H'(-\tau_2)] \rangle, \tag{8}$$

where the square brackets denote a commutator and the angular brackets an ensemble average, and the calculation is done within the interaction picture. The superscripts 1 and 2, as well as the argument of ω or 2ω, indicate first-order and second-order response, respectively.

Following Ref. 33, we obtain the first-order induced dipole moment

$$\langle \delta\vec{p}^{(1)}(\omega) \rangle = \overleftrightarrow{\alpha}(\omega)\cdot\vec{\mathcal{E}}, \tag{9}$$

where the linear microscopic polarizability is

$$\vec{\vec{\alpha}}(\omega)=\alpha_{ij}=\begin{pmatrix}\alpha_{\parallel}(\omega) & 0 & 0\\ 0 & \alpha_{\perp}(\omega) & 0\\ 0 & 0 & \alpha_{\perp}(\omega)\end{pmatrix}, \quad (10)$$

and to emphasize the dependence on each bond's orientation we introduce the notation $\alpha_{\parallel}\leftarrow\alpha_x$ and $\alpha_{\perp}\leftarrow\alpha_y=\alpha_z$ for its parallel and perpendicular response, with

$$\alpha_i(\omega)=\frac{e^2/m}{\omega_i^2-\omega^2} \quad (\text{with } i=\parallel \text{ or } \perp). \quad (11)$$

The linear response of the oscillator is well described by Eq. (9), since the linear quadrupolar and magnetic contributions are negligible in the long-wavelength limit.[33] Likewise, the second-order induced dipole moment is

$$\langle \delta p_i^{(2)}(2\omega)\rangle=[\chi_{ijkl}^{(d)}(\omega)+\chi_{ijkl}^{(m)}(\omega)]\mathcal{E}_j(\nabla_k\mathcal{E}_l), \quad (12)$$

where we adopt Einstein convention on repeated indices. Here,

$$\chi_{ijkl}^{(d)}(\omega)=\frac{1}{2e}[\alpha_{il}(2\omega)\alpha_{jk}(\omega)+\alpha_{ik}(2\omega)\alpha_{jl}(\omega)] \quad (13)$$

and

$$\chi_{ijkl}^{(m)}(\omega)=\frac{3}{2e}[\alpha_{il}(2\omega)\alpha_{jk}(\omega)-\alpha_{ik}(2\omega)\alpha_{jl}(\omega)] \quad (14)$$

are the dipolar electric (d) and magnetic (m) originated contributions to the microscopic second-order susceptibility of the oscillator. Finally, the second-order induced electric quadrupolar moment is

$$\langle \delta Q_{ij}^{(2)}(2\omega)\rangle=\chi_{ijkl}^{(Q)}(\omega)\mathcal{E}_k\mathcal{E}_l, \quad (15)$$

with a microscopic second-order electric quadrupolar (Q) susceptibility given by

$$\chi_{ijkl}^{(Q)}(\omega)=\frac{1}{2e}[\alpha_{il}(\omega)\alpha_{jk}(\omega)+\alpha_{ik}(\omega)\alpha_{jl}(\omega)]. \quad (16)$$

We can show[33] that the microscopic susceptibilities $\vec{\vec{\alpha}}$ and $\vec{\vec{\chi}}^{(d),(m),(Q)}$ of a single oscillator determine all the response functions which are relevant within the long wavelength limit.

It is remarkable that in this model the nonlinear susceptibilities at frequency ω are factorized into simple products of the linear polarizability at ω and 2ω. Hence, from the knowledge of $\alpha_i(\omega)$ we can get completely the microscopic nonlinear behavior.

B. Bonds in a tetrahedron

The semiconductors that we want to study have a simple diamondlike structure, with a tetrahedron as the basic unit. This unit can be viewed as a cube with one atom at the center linked through four bonds to atoms sitting at alternate corners (Fig. 1). The diamond structure is constructed by replicating these four bonds into four intercalated fcc lattices. The polarization induced in the semiconductor originates from the displacement of its charge distribution which typically has strong maxima at the middle of each bond for monatomic semiconductors, with the exception of diamond C,

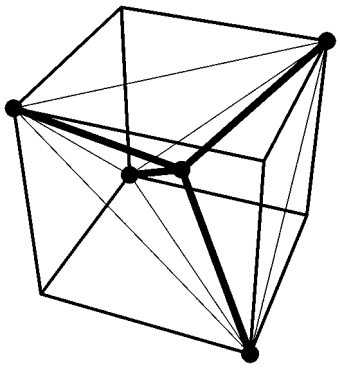

FIG. 1. Illustration of the diamond structure of Si. We show a tetrahedral building block consisting of a cube with Si atoms at alternate vertices joined to another Si atom at the cube's center by four bonds. The crystal can be viewed as an fcc lattice made of replicas of this basic unit.

which has a bimodal distribution. Therefore, we model the response of the semiconductor as that of a lattice of anisotropic cylindrically symmetric polarizable bonds[38] such as those described above. For each bond we introduce a coordinate system centered on it and with the x axis aligned with the symmetry axis. To transform its response to the crystal's coordinate system we simply displace its center and rotate its symmetry axis. We will employ Eqs. (12)–(16) to relate the nonlinear response of each bond to its linear polarizability.

In the bond's coordinate axis the polarizability $\vec{\vec{\alpha}}$ is given by Eq. (10), from which we can build the nonlinear response and then get the corresponding tensor for each bond orientation λ through a rotation,

$$\alpha_{ij}^{\lambda}=\mathcal{R}_{im}^{\lambda}\mathcal{R}_{jn}^{\lambda}\alpha_{mn} \quad (17)$$

and

$$\chi_{ijkl}^{\lambda}=\mathcal{R}_{im}^{\lambda}\mathcal{R}_{jn}^{\lambda}\mathcal{R}_{kr}^{\lambda}\mathcal{R}_{ls}^{\lambda}\chi_{mnrs}, \quad (18)$$

where $\vec{\vec{\chi}}$ refers to any one of the electric dipolar (d) or magnetic dipolar (m) or electric quadrupolar (Q) susceptibility tensors calculated using Eqs. (13), (14), and (16) in the bond's coordinate system. In Eqs. (17) and (18), $\mathcal{R}^{\lambda}$ is the matrix that rotates the λth bond system into the crystal's coordinate system. Alternatively, we could take advantage of the cylindrical symmetry to write

$$\vec{\vec{\alpha}}^{\lambda}=\alpha_{\parallel}\hat{e}^{\lambda}\hat{e}^{\lambda}+\alpha_{\perp}(\mathbb{1}-\hat{e}^{\lambda}\hat{e}^{\lambda}), \quad (19)$$

where $\hat{e}^{\lambda}$ is a unitary vector along the direction of the λth bond. The nonlinear susceptibilities can then be constructed directly in the crystal's system by substituting Eq. (19) into Eqs. (13), (14), and (16).

Based on the microscopic response of each bond, in the following section we will show how to obtain the macroscopic susceptibilities required for the calculation of the SHG conversion efficiency of the crystal.

III. MACROSCOPIC SUSCEPTIBILITIES

In this section we calculate the macroscopic susceptibilities of the semi-infinite diamondlike lattice of polarizable bonds previously described. The susceptibilities are defined

through the macroscopic second-order nonlinear polarization, according to the following standard definitions. For the centrosymmetric bulk, the first nonzero contribution to the second-order nonlinear polarization per unit volume is given by

$$P_i^{(b)}(\vec{r},2\omega)=\chi_{ijkl}^{(b)}E_j(\vec{r},\omega)\nabla_k E_l(\vec{r},\omega), \tag{20}$$

where $\vec{E}(\vec{r},\omega)$ is the fundamental electric field of frequency ω at position $\vec{r}$ within the bulk (b), and $\vec{\vec{\chi}}^{(b)}$ is the bulk second order macroscopic susceptibility. For a cubic system Eq. (20) can be further simplified in the standard cubic axes[13,14]

$$P_i^{(b)}(2\omega)=\gamma\nabla_i(\vec{E}(\vec{r},\omega)\cdot\vec{E}(\vec{r},\omega))+\zeta E_i(\vec{r},\omega)\nabla_i E_i(\vec{r},\omega)$$
$$\text{(no summation)}, \tag{21}$$

where we assumed a single transverse plane wave in the bulk so that $\nabla\cdot\vec{E}=0$ and $\vec{E}\cdot\nabla=0$. Here,

$$\zeta=\chi_{iiii}^{(b)}-\chi_{ijij}^{(b)}-\chi_{ijji}^{(b)}-\chi_{iijj}^{(b)} \quad \text{(no summation and } i\neq j) \tag{22}$$

yields the anisotropic behavior of SHG coming from the bulk, and

$$\gamma=\frac{1}{2}\chi_{ijij}^{(b)} \quad \text{(no summation and } i\neq j) \tag{23}$$

gives the corresponding isotropic bulk contribution.

The lack of inversion symmetry at the surface (s) allows us to write an effective singular polarization $\mathcal{P}_i^{(s)}(2\omega)\,\delta(z-z_0)$ which, following Refs. 13 and 14, we locate in vacuum just on top of the semi-infinite crystal $(z=z_{0^-})$, and whose dipole moment per unit area is given by

$$\mathcal{P}_i^{(s)}(2\omega)=\chi_{ijk}^{(s)}(\omega)E_j(B,\omega)E_k(B,\omega), \tag{24}$$

where $\vec{\vec{\chi}}^{(s)}$ is the second order macroscopic surface susceptibility, and $\vec{E}(B,\omega)$ is the macroscopic electric field just below the selvedge ($z=z_{0^+}$ within the long wavelength approximation) which differs from the field just on top $\vec{E}(A,\omega)$ due to screening, i.e.,

$$\vec{E}(B,\omega)=(E_x(A,\omega),E_y(A,\omega),E_z(A,\omega)/\epsilon(\omega)), \tag{25}$$

with $\epsilon(\omega)$ the isotropic bulk dielectric function. Here we have chosen a coordinate system such that the surface lies at $z=z_0$ and $z>z_0$ is inside the system. Notice that the coordinate system employed in the surface calculation might differ from the standard cubic system employed in the bulk calculation above. Due to the surface symmetry there are only a few nonzero independent components of the surface susceptibility, namely, $\chi_{zzz}^{(s)}$, $\chi_{zzx}^{(s)}=\chi_{zzy}^{(s)}$, and $\chi_{zxx}^{(s)}=\chi_{zyy}^{(s)}$ for the (001) face, $\chi_{zzz}^{(s)}$, $\chi_{zzx}^{(s)}\neq\chi_{zzy}^{(s)}$, and $\chi_{zxx}^{(s)}\neq\chi_{zyy}^{(s)}$ for the (110) face, and $\chi_{zzz}^{(s)}$, $\chi_{zzx}^{(s)}=\chi_{zzy}^{(s)}$, $\chi_{zxx}^{(s)}=\chi_{zyy}^{(s)}$, and $\chi_{xxx}^{(s)}=-\chi_{xyy}^{(s)}=-\chi_{yyx}^{(s)}$ for the (111) face. There is an overall permutation symmetry in the last two indices, i.e., $\chi_{ijk}^{(s)}=\chi_{ikj}^{(s)}$, and the susceptibilities of different faces are in general different.

We mention that for the diamond structure we may obtain other nonzero components of $\vec{\vec{\chi}}^{(s)}$ since the *microscopic* symmetry of a face may be less than the *macroscopic* symmetry. For example, the (001) face has on the average the same symmetry as a square, which yields the nonzero components described above. However, if we look at a microscopic region, the displacement between the first and second crystalline planes might have a component along a square diagonal, say the $[110]$ direction, which would therefore be inequivalent to the second diagonal along the $[1\bar{1}0]$ direction. This allows a nonzero value for $\chi_{zxy}^{(s)}$. Nevertheless, any surface has steps, so that on other microscopic regions the roles of the $[110]$ and $[1\bar{1}0]$ directions are reversed, and so is the sign of $\chi_{zxy}^{(s)}$. It is only after averaging over both kinds of regions, that is, over the macroscopic region being illuminated by the beam, that the contribution to the surface polarization coming from $\chi_{zxy}^{(s)}$ cancels out, regaining the full symmetry of the square as if $\chi_{zxy}^{(s)}=0$.[14]

With the knowledge of γ, ζ, and $\vec{\vec{\chi}}^{(s)}$ it is a simple matter to calculate the SHG radiated efficiency following Refs. 13 and 14. Therefore, in the rest of this section, we develop the formalism based on the polarazible bonds (Sec. II) in order to calculate the macroscopic susceptibilities.

A. Linear response

We look for the first order induced dipole moment of every bond $n\lambda$, where n denotes a site of the fcc lattice corresponding to the λth bond orientation. To simplify our notation we substitute

$$\langle\delta\vec{p}^{(1)}(\omega)\rangle\rightarrow\vec{p}_{n\lambda}(\omega), \tag{26}$$

and we adopt a convention in which an argument of *only* one ω implies first order. The linear polarization $\vec{p}_{n\lambda}$ obeys, in analogy to Eq. (9),

$$\vec{p}_{n\lambda}(\omega)=\vec{\vec{\alpha}}^{\lambda}(\omega)\cdot\vec{\mathcal{E}}_{n\lambda}, \tag{27}$$

where

$$\vec{\mathcal{E}}_{n\lambda}=\vec{E}^{(\text{ext})}(\vec{r}_{n\lambda})+\sum_{n'\lambda'}\vec{\vec{M}}_{n\lambda n'\lambda'}\cdot\vec{p}_{n'\lambda'}(\omega) \tag{28}$$

is the local field, which is the sum of the external field $\vec{E}^{(\text{ext})}(\vec{r}_{n\lambda})$ and the dipolar field produced by all other bonds. The tensor

$$\vec{\vec{M}}_{n\lambda n'\lambda'}=\nabla\nabla\frac{1}{|\vec{r}-\vec{r}_{n'\lambda'}|}\Big|_{\vec{r}=\vec{r}_{n\lambda}} \tag{29}$$

yields the dipolar interaction between the bonds $n\lambda$ and $n'\lambda'$. The sum in Eq. (28) is over all bonds $n'\lambda'\neq n\lambda$ and can be carried out using standard planewise schemes (see, for instance, Ref. 41). For this task we write $\vec{r}_{n\lambda}=(\vec{R}_{\ell\nu\lambda},z_{\ell\lambda})$, where $\ell\lambda$ denotes the ℓth crystal plane of λ bonds at position $z=z_{\ell\lambda}$ and ν numbers the individual bonds that make up this plane, so that $\vec{R}_{\ell\nu\lambda}$ spans a 2D periodic lattice for each ℓ. Assuming the long wavelength approximation, the polarization of all bonds λ that belong to a given plane ℓ is the same, $\vec{p}_{\ell\nu\lambda}=\vec{p}_{\ell\lambda}$, so we can sum over ν' and obtain from Eq. (27) that

$$\vec{p}_{\ell\lambda}(\omega)=\overleftrightarrow{\alpha}^{\lambda}(\omega)\cdot\left(\vec{E}(A,\omega)+\sum_{\ell'\lambda'}\overleftrightarrow{\mathcal{M}}_{\ell\lambda\ell'\lambda'}\cdot\vec{p}_{\ell'\lambda'}(\omega)\right), \tag{30}$$

where we neglect the slow spatial dependence of $\vec{E}^{(\mathrm{ext})}\times(\vec{r}_{n\lambda})\rightarrow\vec{E}(A,\omega)$ and we introduce the interplane interactions

$$\overleftrightarrow{\mathcal{M}}_{\ell\lambda\ell'\lambda'}=\sum_{\nu'}{}'\overleftrightarrow{M}_{\ell\nu\lambda\ell'\nu'\lambda'}. \tag{31}$$

Here the prime indicates that the self-interaction of a bond is excluded from the sum, i.e., the term with $\nu=\nu'$ when both $\ell=\ell'$ and $\lambda=\lambda'$. It turns out the $\overleftrightarrow{\mathcal{M}}$ decays exponentially as $|\ell-\ell'|$ increases. The solution of Eq. (30) gives the linear polarization of the ℓth plane for each bond λ, so that the total polarization is simply given by

$$\vec{p}_{\ell}(\omega)=\sum_{\lambda}\vec{p}_{\ell\lambda}(\omega). \tag{32}$$

Later on we will require the local field $\vec{\mathcal{E}}_{\ell\lambda}$ at the λth bonds of the ℓth plane, which can be obtained from Eqs. (27) and (30),

$$\vec{\mathcal{E}}_{\ell\lambda}(\omega)=(\overleftrightarrow{\alpha}^{\lambda}(\omega))^{-1}\cdot\vec{p}_{\ell\lambda}(\omega), \tag{33}$$

once Eq. (30) has been solved for $\vec{p}_{\ell\lambda}$.

Now we consider the bulk of the system. We have that $\vec{p}_{\ell\lambda}(\omega)\rightarrow\vec{p}_{\lambda}(B,\omega)$ is independent of the plane number ℓ, so that Eq. (30) reduces to

$$\sum_{\lambda'}[\mathbb{1}\delta_{\lambda\lambda'}-\overleftrightarrow{\alpha}^{\lambda}(\omega)\cdot\overleftrightarrow{\mathcal{U}}_{\lambda\lambda'}]\cdot\vec{p}_{\lambda'}(B,\omega)=\overleftrightarrow{\alpha}^{\lambda}(\omega)\cdot\vec{E}(A,\omega), \tag{34}$$

where the interaction between bond types λ and λ' is given by the $[(4\times3)\times(4\times3)]$ matrix

$$\overleftrightarrow{\mathcal{U}}_{\lambda\lambda'}=\sum_{\ell'=-\infty}^{\infty}\overleftrightarrow{\mathcal{M}}_{\ell\lambda\ell'\lambda'}. \tag{35}$$

The solution of Eq. (34) gives the linearly induced bulk dipole moment of each bond and therefore the total bulk dipole moment is given by

$$\vec{P}(B,\omega)=n_b\sum_{\lambda}\vec{p}_{\lambda}(B,\omega) \tag{36}$$

with n_b the 3D density of bonds. Finally, we identify the isotropic bulk dielectric response $\epsilon(\omega)$ through

$$\vec{P}(B,\omega)=\frac{\epsilon(\omega)-1}{4\pi}\vec{E}(B,\omega). \tag{37}$$

Since $\vec{P}(B,\omega)$ is a function of $\overleftrightarrow{\alpha}$, Eq. (37) yields an analytical expression which relates $\epsilon(\omega)$ to the principal polarizabilities $\alpha_{\parallel}$ and $\alpha_{\perp}$. This relation is a generalization of the Clausius-Mossotti (CM) relation to the diamond structure.

B. Surface nonlinear response

We consider now the second order dipole moments. First we confine our attention to the surface region where the local field has a large uncompensated gradient at each bond site of order $\nabla\approx1/a$ with a the lattice parameter. Later we will calculate the polarization at the bulk where there is a cancellation that leaves only small gradients of order $\nabla\approx\omega/c$.

The equation for the total second-order dipole moment near the surface is given by

$$\vec{p}^{(\mathrm{tot})}_{n\lambda}(2\omega)=\vec{p}^{(\mathrm{nl})}_{n\lambda}(2\omega)+\overleftrightarrow{\alpha}^{\lambda}(2\omega)\cdot\left[\vec{\mathcal{E}}^{(Q)}_{n\lambda}(2\omega)+\sum_{n'\lambda'}\overleftrightarrow{M}_{n\lambda n'\lambda'}\cdot\,p^{(\mathrm{tot})}_{n'\lambda'}(2\omega)\right]. \tag{38}$$

Here, the total dipole moment at 2ω is driven by the nonlinear response to the spatially varying linear local field which we obtain from Eq. (12),

$$\langle\delta p^{(2)}_i(2\omega)\rangle\rightarrow(\vec{p}^{(\mathrm{nl})}_{n\lambda}(2\omega))_i=\chi^{(d),\lambda}_{ijkl}(\vec{\mathcal{E}}_{n\lambda}(\omega))_j\nabla_l(\vec{\mathcal{E}}_{n\lambda}(\omega))_k. \tag{39}$$

Notice that near the surface $(\omega/c)B\ll\nabla E\approx E/a$, so we have ignored the magnetic contribution to the λth's bond susceptibility $\overleftrightarrow{\chi}^{(m),\lambda}$ [see Eq. (18)]. However, this magnetic contribution will be included when we calculate the nonlinear bulk response below. The second-order dipole moment is also driven by the linear response to the field at 2ω due to the oscillating quadrupoles [Eq. (15)],

$$(\vec{\mathcal{E}}^{(Q)}_{n\lambda}(2\omega))_i=\frac{1}{2}\sum_{n'\lambda'}(\overleftrightarrow{N}_{n\lambda n'\lambda'})_{ijk}(\overleftrightarrow{Q}^{(\mathrm{nl})}_{n'\lambda'}(2\omega))_{jk}. \tag{40}$$

Finally, the last term on the left-hand side of Eq. (38) represents the linear response to the field at 2ω due to the other dipoles oscillating at 2ω and should be included to achieve self-consistency.

In Eq. (39) we require the gradient of the local field evaluated at the bonds, which turns out to be proportional to the linear dipole moment and is given by[33]

$$\nabla_i(\vec{\mathcal{E}}_{n\lambda}(\omega))_j=-\sum_{n'\lambda'}(\overleftrightarrow{N}_{n\lambda n'\lambda'})_{ijk}(\vec{p}_{n'\lambda'}(\omega))_k, \tag{41}$$

with

$$\overleftrightarrow{N}_{n\lambda n'\lambda'}=-\nabla\nabla\nabla\frac{1}{|\vec{r}-\vec{r}_{n'\lambda'}|}\bigg|_{\vec{r}=\vec{r}_{n\lambda}} \tag{42}$$

being the same tensor as in Eq. (40). We also require the nonlinear induced quadrupolar moment given by Eq. (15), and rewritten as

$$\langle\delta Q^{(2)}_{ij}(2\omega)\rangle\rightarrow(\overleftrightarrow{Q}^{(\mathrm{nl})}_{n\lambda}(2\omega))_{ij}=\chi^{(Q),\lambda}_{ijkl}(\omega)(\vec{\mathcal{E}}_{n\lambda}(\omega))_k(\vec{\mathcal{E}}_{n\lambda}(\omega))_l \tag{43}$$

with $\overleftrightarrow{\chi}^{(Q),\lambda}$ the microscopic quadrupolar susceptibility of the λth bond [see Eq. (18)].

We apply the same planewise summation scheme to Eq. (38) that led to Eq. (30) by defining

$$\vec{\mathcal{N}}_{\ell\lambda\ell'\lambda'}=\sum_{\nu}{}'\vec{N}_{\ell\nu\lambda\ell'\nu'\lambda'}, \tag{44}$$

and writing

$$\sum_{\lambda'\ell'}[\mathbb{1}\delta_{\lambda\lambda'}\delta_{\ell\ell'}-\vec{\alpha}^{\lambda}(2\omega)\cdot\vec{\mathcal{M}}_{\ell\lambda\ell'\lambda'}]\cdot\vec{p}^{(\mathrm{tot})}_{\ell'\lambda'}(2\omega)=\vec{\mathcal{S}}_{\ell\lambda}(2\omega), \tag{45}$$

where $\vec{\mathcal{S}}$ is the nonlinear source,

$$\begin{aligned}(\vec{\mathcal{S}}_{\ell\lambda}(2\omega))_i=&-\chi^{(d),\lambda}_{ijkl}(\vec{\mathcal{E}}_{\ell\lambda}(\omega))_j\sum_{\lambda',\ell'}(\vec{\mathcal{N}}_{\ell\lambda\ell'\lambda'})_{klm}\\&\times(\vec{p}_{\ell'\lambda'}(\omega))_m\\&+\frac{1}{2}\alpha^{\lambda}_{ij}(2\omega)\sum_{\lambda',\ell'}(\vec{\mathcal{N}}_{\ell\lambda\ell'\lambda'})_{jkl}\chi^{(Q),\lambda'}_{klmn}\\&\times(\vec{\mathcal{E}}_{\ell'\lambda'}(\omega))_m(\vec{\mathcal{E}}_{\ell'\lambda'}(\omega))_n.\end{aligned} \tag{46}$$

Notice that the driving fields for $\vec{\mathcal{S}}$ depend on the linear local field $\vec{\mathcal{E}}_{\ell\lambda}(\omega)$ and the linear dipole moment $\vec{p}_{\ell\lambda}(\omega)$, which are related through Eq. (33). The interaction $\vec{\mathcal{N}}_{\ell\lambda\ell'\lambda'}$ decays very quickly as the separation between planes increases. Therefore, as we move away from the surface ($\ell=0$) into the bulk ($\ell\to\infty$), the driving source $\vec{\mathcal{S}}$ becomes negligible, so $\vec{p}^{(\mathrm{tot})}_{\ell\lambda}(2\omega)$ vanishes as $\ell\to\infty$ and the total surface-dipole moment per unit area

$$\vec{\mathcal{P}}^{(s)}(2\omega)=n_s\sum_{\ell,\lambda}\vec{p}^{(\mathrm{tot})}_{\ell\lambda}(2\omega) \tag{47}$$

is well defined. Here, n_s is the number of bonds per unit area. In order to obtain the different components of the surface susceptibility tensor $\vec{\vec{\chi}}^{(s)}$ from this equation, we fix in turn the driving field $\vec{E}(A,\omega)$ [see Eq. (25)] along different directions. Indeed, to get $\chi^{(s)}_{ijj}$ we choose $\vec{E}(A)$ along the j direction. Thus, we would generate $\chi^{(s)}_{ixx}$, $\chi^{(s)}_{iyy}$, and $\chi^{(s)}_{izz}$, with $i=x$, y, or z. If we now chose $\vec{E}(B)$ with two null components, say $E_j(B)$ and $E_k(B)$ for mutually orthogonal directions $j\neq k$, we would get

$$\mathcal{P}^{(s)}_i=\chi^{(s)}_{ijj}E_j(B)^2+\chi^{(s)}_{ikk}E_k(B)^2+2\chi^{(s)}_{ijk}E_j(B)E_k(B). \tag{48}$$

Knowing $\chi^{(s)}_{ijj}$ and $\chi^{(s)}_{ikk}$, we can solve this equation for $\chi^{(s)}_{ijk}$, henceforth generating $\chi^{(s)}_{ixy}$, $\chi^{(s)}_{ixz}$, and $\chi^{(s)}_{iyz}$ for $i=x$, y, or z. It should be clear from Eq. (24) that $\chi^{(s)}_{ijk}=\chi^{(s)}_{ikj}$, and then all 27 components of $\vec{\vec{\chi}}^{(s)}$ are finally obtained. We recall that some of the non-null components found through this procedure are forbidden by the *macroscopic* symmetry of the surface; they would become zero after averaging over the inequivalent top surface layers,[14] and they should be ignored in the calculation of the SHG signal.

C. Bulk nonlinear response

Now, we consider the bulk (B) nonlinear induced-dipole polarization $\vec{p}^{(\mathrm{tot})}_{\lambda}(B,2\omega)$ and $\vec{p}^{(\mathrm{nl})}_{\lambda}(B,2\omega)$. In the long wavelength regime they are very slowly dependent on position, so that following the classical local-field argument, the total bulk quadratic-dipole polarization obeys

$$\sum_{\lambda'}[\mathbb{1}\delta_{\lambda\lambda'}-\vec{\alpha}^{\lambda}(2\omega)\cdot\vec{\mathcal{U}}_{\lambda\lambda'}]\cdot\vec{p}^{(\mathrm{tot})}_{\lambda'}(B,2\omega)=\vec{p}^{(\mathrm{nl})}_{\lambda}(B,2\omega)+\vec{\alpha}^{\lambda}(2\omega)\cdot\vec{\mathcal{E}}^{(Q)}_{\lambda}(B,2\omega). \tag{49}$$

Since now we are in the retarded regime, we have to incorporate the magnetic contribution to the nonlinear polarization,

$$\begin{aligned}(\vec{p}^{(\mathrm{nl})}_{\lambda})_i=&\chi^{(d),\lambda}_{ijkl}(\omega)(\vec{\mathcal{E}}_{\lambda}(B,\omega))_j\nabla_k(\vec{\mathcal{E}}_{\lambda}(B,\omega))_l\\&+\chi^{(m),\lambda}_{ijkl}(\omega)(\vec{\mathcal{E}}_{\lambda}(B,\omega))_j\nabla_k(\vec{E}(B,\omega))_l.\end{aligned} \tag{50}$$

The first term on the right-hand side is the electric-dipole-driven term, proportional to the gradient of the local electric field, and the second term corresponds to the magnetic-dipole-driven term. Notice that in the latter we made the substitution $\vec{\mathcal{E}}_{\lambda}(B)\to\vec{E}(B)$ since the spatial fluctuations of the transverse fields are of order $(a\omega/c)^2$ times smaller than the corresponding fluctuations of the longitudinal electric field.[42]

For a strictly space-independent field the source terms in Eq. (49) would be null. To calculate them we have to account for the weak spatial variation of both the long-range bulk-field and its short-range local-field corrections. Therefore, we assume a plane-wave spatial variation of the form

$$\vec{\mathcal{E}}_{\ell\nu\lambda}(\omega)=\vec{\mathcal{E}}_{\lambda}(B,\omega)e^{i\vec{q}\cdot\vec{r}_{\ell\nu\lambda}}, \tag{51}$$

for the linear fields and for the polarization, where the linear local field may be obtained from Eqs. (33) and (34), and we allow the small wave vector $\vec{q}$ to point in any direction. Therefore, the fields depend not only on the plane index ℓ but also on the in-plane index ν.

We start with the quadrupolar field

$$\begin{aligned}(\vec{\mathcal{E}}^{(Q)}_{\ell\nu\lambda}(2\omega))_i\equiv&(\vec{\mathcal{E}}^{(Q)}_{\lambda}(B,2\omega)_ie^{2i\vec{q}\cdot\vec{r}_{\ell\nu\lambda}})\\&=\frac{1}{2}\sum_{\ell'\nu'\lambda'}(\vec{\vec{N}}_{\ell\nu\lambda\ell'\nu'\lambda'})_{ijk}(\vec{Q}^{(nl)}_{\ell'\nu'\lambda'})_{jk},\end{aligned} \tag{52}$$

where the quadrupole moment is given by Eq. (43). Using Eq. (51), and assuming that $|\vec{q}\cdot\Delta\vec{r}_{\ell\nu\lambda\ell'\nu'\lambda'}|\ll1$, for all the terms $\ell'\nu'$ that contribute to the sum in Eq. (52), where $\Delta\vec{r}_{\ell\nu\lambda\ell'\nu'\lambda'}\equiv\vec{r}_{\ell\nu\lambda}-\vec{r}_{\ell'\nu'\lambda'}$, we get for any plane ℓ in the bulk the following expansion for the quadrupolar field to first order in $\vec{q}\cdot\Delta\vec{r}_{\ell\nu\lambda\ell'\nu'\lambda'}$:

$$(\vec{\mathcal{E}}^{(Q)}_{\lambda}(B,2\omega))_i=\frac{1}{2}\sum_{\ell'\nu'\lambda'}(\overleftrightarrow{N}_{\ell\nu\lambda\ell'\nu'\lambda'})_{ijk}(\overleftrightarrow{Q}^{(\mathrm{nl})}_{\lambda'}(B,2\omega))_{jk}e^{2i\vec{q}\cdot\Delta\vec{r}_{\ell\nu\lambda\ell'\nu'\lambda'}}$$

$$\simeq\frac{1}{2}\sum_{\lambda'}\left[\left(\sum_{\ell'\nu'}(\overleftrightarrow{N}_{\ell\nu\lambda\ell'\nu'\lambda'})_{ijk}\right)+2i(\vec{q})_l\left(\sum_{\ell'\nu'}(\Delta\vec{r}_{\ell\nu\lambda\ell'\nu'\lambda'})_l(\overleftrightarrow{N}_{\ell\nu\lambda\ell'\nu'\lambda'})_{ijk}\right)\right](\overleftrightarrow{Q}^{(\mathrm{nl})}_{\lambda'}(B,2\omega))_{jk}$$

$$\equiv\sum_{\lambda'}(\overleftrightarrow{\eta}_{\lambda\lambda'})_{ijkl}(\overleftrightarrow{Q}^{(\mathrm{nl})}_{\lambda'}(B,2\omega))_{jk}(iq_l), \tag{53}$$

where the first term on the second line is zero in view of the odd parity of $\overleftrightarrow{N}$ and the bulk quadrupolar amplitude is

$$(\overleftrightarrow{Q}^{(\mathrm{nl})}_{\lambda}(B,2\omega))_{ij}=\chi^{(Q),\lambda}_{ijkl}(\omega)(\vec{\mathcal{E}}_{\lambda}(B,\omega))_k(\vec{\mathcal{E}}_{\lambda}(B,\omega))_l. \tag{54}$$

Here, we introduced the fourth rank quadrupole-dipole interaction tensor

$$(\overleftrightarrow{\eta}_{\lambda\lambda'})_{ijkl}=\sum_{\ell'\nu'}(\overleftrightarrow{N}_{\ell\nu\lambda\ell'\nu'\lambda'})_{ijk}(\Delta\vec{r}_{\ell\nu\lambda\ell'\nu'\lambda'})_l. \tag{55}$$

This tensor is most easily evaluated in the cubic axis making use of the permutation symmetry of cubic crystals,

$$(\overleftrightarrow{\eta}_{\lambda\lambda'})_{ijkl}=\sum_{\ell'=-\infty}^{\infty}\left(\sum_{\nu'}(\overleftrightarrow{N}_{\ell\nu\lambda\ell'\nu'\lambda'})_{i'j'k'}\right)(z_{\ell\lambda}-z_{\ell'\lambda'})$$

$$=\sum_{\ell'}(\overleftrightarrow{\mathcal{N}}_{\ell\lambda\ell'\lambda'})_{i'j'k'}(z_{\ell\lambda}-z_{\ell'\lambda'}), \tag{56}$$

where the indices $i'j'k'z$ are obtained from $ijkl$ by performing a cyclic permutation.[33]

Following a similar treatment for the dipolar term of Eqs. (49) and (50) we obtain the gradient of the local field that accompanies a plane wave propagating within the bulk,[33]

$$\nabla_i(\vec{\mathcal{E}}_{\lambda}(B,\omega))_j=i(\vec{q})_i(\vec{E}(B,\omega))_j$$

$$-i(\vec{q})_l\sum_{\lambda'}(\overleftrightarrow{\eta}_{\lambda\lambda'})_{ijkl}(\vec{p}_{\lambda'}(B,\omega))_k, \tag{57}$$

where the first term gives the variation of the long-range bulk field, and the second term gives the short-range local-field corrections.

Now that we have all the terms required for Eq. (49), we proceed to find its solution. First, we define

$$\overleftrightarrow{T}_{\lambda\lambda'}(n\omega)=\mathbb{1}\delta_{\lambda\lambda'}-\overleftrightarrow{\alpha}^{\lambda}(n\omega)\cdot\overleftrightarrow{\mathcal{U}}_{\lambda\lambda'}, \tag{58}$$

with $n=1$ or 2. From Eq. (34) we obtain the amplitude of the bulk linear dipole moment

$$\vec{p}_{\lambda}(B,\omega)=\vec{\wp}^{\lambda}(\omega)\cdot\vec{E}(B,\omega), \tag{59}$$

in terms of the macroscopic linear field, with

$$\vec{\wp}^{\lambda}(\omega)=\sum_{\lambda'}(\overleftrightarrow{T}^{-1}(\omega))_{\lambda\lambda'}\cdot\vec{\alpha}_{\lambda'}(\omega), \tag{60}$$

and from Eq. (33) we get the bulk local field

$$\vec{\mathcal{E}}_{\lambda}(B,\omega)=\overleftrightarrow{\xi}^{\lambda}(\omega)\cdot\vec{E}(B,\omega), \tag{61}$$

with

$$\overleftrightarrow{\xi}^{\lambda}(\omega)=(\overleftrightarrow{\alpha}^{-1}(\omega))^{\lambda}\cdot\overleftrightarrow{\wp}_{\lambda}(\omega). \tag{62}$$

Now, from Eq. (49) we obtain the nonlinear polarization

$$\vec{p}^{(\mathrm{tot})}_{\lambda}(B,2\omega)=\sum_{\lambda'}(\overleftrightarrow{T}^{-1}(2\omega))_{\lambda\lambda'}\cdot\vec{\mathcal{S}}^{\lambda'}(B,2\omega), \tag{63}$$

in terms of the bulk source

$$\mathcal{S}^{\lambda}_i(B,2\omega)=\Gamma^{\lambda}_{ijkl}E_j(B,\omega)\nabla_kE_l(B,\omega), \tag{64}$$

with

$$\Gamma^{\lambda}_{ijkl}=(\chi^{(d),\lambda}_{imkl}+\chi^{(m),\lambda}_{imkl})\xi^{\lambda}_{mj}+(\chi^{(d),\lambda}_{imns}+\chi^{(m),\lambda}_{imns})$$

$$\times\xi^{\lambda}_{mj}\sum_{\lambda'}(\overleftrightarrow{\eta}_{\lambda\lambda'})_{nsrk}\wp^{\lambda'}_{rl}(\omega)$$

$$-\alpha^{\lambda}_{im}(2\omega)\sum_{\lambda'}(\overleftrightarrow{\eta}_{\lambda\lambda'})_{mnsk}\chi^{(Q),\lambda'}_{nsrt}\xi^{\lambda'}_{rj}(\omega)\xi^{\lambda'}_{tl}(\omega). \tag{65}$$

The first (second) term on the right-hand side of Eq. (65) comes from the first (second) term of Eq. (57), whereas the last line comes from the quadrupolar field of Eq. (53). The total bulk polarization per unit volume is written as

$$\vec{P}^{(b)}(2\omega)=n_b\sum_{\lambda}\vec{p}^{(\mathrm{tot})}_{\lambda}(B,2\omega). \tag{66}$$

Comparing Eq. (66) to Eq. (20) we identify the macroscopic bulk susceptibility

$$\overleftrightarrow{\chi}^{(b)}(\omega)=\sum_{\lambda,\lambda'}(\overleftrightarrow{T}^{-1}(2\omega))_{\lambda\lambda'}\cdot\overleftrightarrow{\Gamma}^{\lambda'}(\omega) \tag{67}$$

from which ζ and γ can be obtained using Eqs. (22) and Eq. (23), respectively.

D. Higher multipoles

We conclude our calculation of the nonlinear surface and bulk nonlinear susceptibilities by incorporating the effect of higher induced multipoles to the polarization, namely, by adding the gradient of the quadrupolar density to the dipolar density.[43] The surface polarization becomes[44,45]

$$\mathcal{P}_i^{(s)} \rightarrow \mathcal{P}_i^{(s)} - \frac{1}{2} n_b \sum_\lambda \left(\vec{\vec{Q}}_\lambda(B,2\omega)\right)_{iz}, \tag{68}$$

changing the surface susceptibility to

$$\chi_{ijk}^{(s)} \rightarrow \chi_{ijk}^{(s)} - \frac{1}{2} \tilde{\chi}_{ijk}, \tag{69}$$

where

$$\tilde{\chi}_{ijk} = \sum_\lambda \chi_{izmn}^{(Q),\lambda} \xi_{mj}^\lambda \xi_{nk}^\lambda. \tag{70}$$

Notice that this quadrupolar contribution to the surface polarization is bulk originated. Similarly, we include the effect of higher induced multipoles to the effective bulk polarization,[43]

$$\vec{P}^{(b)}(2\omega) \rightarrow \vec{P}^{(b)}(2\omega) - \frac{1}{2} n_b \sum_\lambda \vec{\vec{Q}}_\lambda(B,2\omega) \cdot (2i\vec{q}), \tag{71}$$

modifying the bulk susceptibility tensor,

$$\chi_{ijkl}^{(b)} \rightarrow \chi_{ijkl}^{(b)} - \tilde{\chi}_{ijkl}, \tag{72}$$

with

$$\tilde{\chi}_{ijkl} = \sum_\lambda \chi_{ikmn}^{(Q),\lambda} \xi_{mj}^\lambda \xi_{nl}^\lambda. \tag{73}$$

We mention that had we used a simple fcc lattice of isotropic polarizable entities (tetrahedra) instead of four interpenetrated lattices of anisotropic polarizable bonds considered above, we would have obtained only one independent component of $\vec{\vec{\chi}}^{(b)}$ corresponding to γ, and thus under these assumption the nonlinear bulk response would have been isotropic. However, although in our model all the bonds are identical except for their orientation, and their response is harmonic-oscillator-like, their anisotropy combined with the lower symmetry of the tetrahedral structure yields $\zeta \neq 0$, rendering the bulk anisotropic.

IV. RESULTS

In the preceding section we obtained the macroscopic nonlinear bulk and surface susceptibilities in terms of the microscopic susceptibility tensors of each bond. Assuming an anisotropic harmonic oscillator model the latter were written [Eqs. (13), (14), and (16)] in terms of the linear polarizabilities $\vec{\vec{\alpha}}^\lambda$. In the following, we assume these relations to hold approximately for the bond susceptibilities of a Si crystal and further assume that $\vec{\vec{\alpha}}^\lambda$ is independent of position. Therefore, in our model we incorporate only the surface modification to the local fields, and we ignore any other surface modification to the linear and nonlinear response such as those due to transitions involving surface states. As discussed at the end of Sec. III A, we can find an expression which relates the bulk dielectric function $\epsilon(\omega)$ to the principal polarizabilities $\alpha_\parallel(\omega)$ and $\alpha_\perp(\omega)$, which is a generalization of the Clausius-Mossotti (CM) relation to the diamond structure. Close to the visible spectral region, we expect that the main contributions to $\alpha_\parallel$ originate in bonding-antibonding transitions, while $\alpha_\perp$ is due to transitions involving atomic states with different symmetry. We assume the latter have larger resonant frequencies than the former, and thus we approximate $\alpha_\perp(\omega)$ by a Lorentzian centered at some relatively high frequency $\omega_\perp$ with a weight characterized by a frequency parameter ω_p, i.e.,

$$\alpha_\perp(\omega) = \frac{\omega_p^2}{\omega_\perp^2 - \omega^2}. \tag{74}$$

After choosing these parameters, we solve the generalized CM relation for each frequency to obtain $\alpha_\parallel(\omega)$ in terms of the experimentally measured bulk dielectric function $\epsilon(\omega)$.[46] Having determined the polarizability tensor, and therefore also the nonlinear susceptibilities (Sec. II), we solve the local field equations to obtain first the linear dipole moments $\vec{p}_{n\lambda}(\omega)$ (Sec. III A), then $\vec{p}_{n\lambda}^{(nl)}(2\omega)$, $\vec{\vec{Q}}_{n\lambda}^{(nl)}(2\omega)$, and the total nonlinear dipole moments $\vec{p}_{n\lambda}^{(\mathrm{tot})}(2\omega)$ (Sec. III B and Sec. III C). Next, we obtain the bulk and surface polarizations $\vec{P}^{(b)}(2\omega)$ and $\vec{\mathcal{P}}^{(s)}(2\omega)$ per unit volume and unit area, respectively, and the nonlinear surface and bulk susceptibilities. The SHG efficiency $\mathcal{R}(\omega)$ is defined through

$$\mathcal{R}(\omega) = \frac{I_r(2\omega)}{I_i^2(\omega)}, \tag{75}$$

where $I_r(2\omega)$ is the reflected intensity of the SH field, and $I_i(\omega)$ is the incident intensity of the fundamental field. It can finally be calculated in terms of the nonlinear susceptibilities using standard formulas.[13,14]

The anisotropy of the SHG of Si(111) and Si(001) has been measured for all possible combinations of incoming and outgoing s and p polarizations at $\hbar\omega = 1.17$ eV and 2.34 eV.[2–5] For the following results, we chose the parameters $\hbar\omega_\perp = 7.17$ eV and $\hbar\omega_p = 1.68$ eV. These were obtained by fitting the ratio between the heights of the peaks observed in the azimuthal angular dependence of $\mathcal{R}_{sp}$ for p polarized outgoing and s polarized incoming light upon a Si(111) surface for both frequencies. As will be shown below, with these parameters we obtain a good agreement with the other anisotropy measurements performed at the fixed frequencies above. Our value of $\omega_\perp$ is of the order of the transition energy between the atomic states of Si $3p^2 {}^3P$ with $J=0$ and $3d^3 D^0$ with $J=1$,[47] in qualitative agreement with the discussion before Eq. (74). We achieved a good numerical convergence using 40 crystalline planes in the calculation and including a small imaginary part in $\alpha_\perp$ by adding a damping frequency $\omega_c \ll \omega_\perp$ in the Lorentzian (74); we took $\omega_c = 0.1$ eV, although its actual value is not very important as long as it is small.

A. Linear and nonlinear anisotropy

In this section we present the results obtained for the reflectance anisotropy of Si(110) and the SHG anisotropy for Si(001) and Si(111).

In Fig. 2, we show a plot of $\alpha_\parallel$ vs ω, obtained from the generalized CM relation through the procedure described above. We observe the usual peaks due to the singularities of the bulk joint density of states, although they are substantially shifted due to short range Coulomb and exchange in-

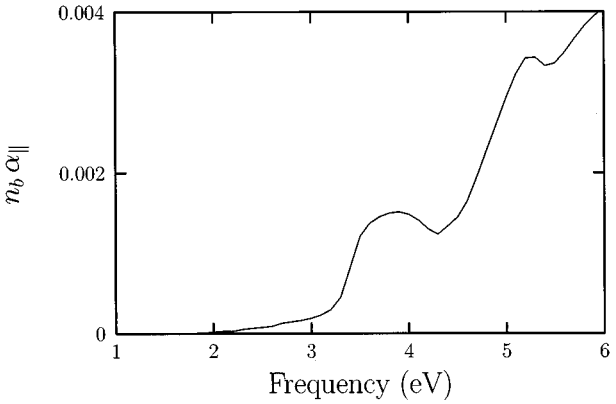

FIG. 2. Imaginary part of the axial bond polarizability $\alpha_\parallel$ of Si as a function of frequency ω. The structure appears substantially shifted from the singularities of the joint density of states due to short range Coulomb and exchange interactions, which are compensated within the bulk by the long range local field effect.

teractions. We recall that the bulk local field effect induces an almost equal but opposite shift.[48] With this fitted $\alpha_\parallel(\omega)$ and taking $\alpha_\perp(\omega)$ from Eq. (74), we calculated the surface induced anisotropy[37] $\Delta R/R$ of the linear normalized reflectance of Si(110), where $\Delta R = R_{1\bar{1}0} - R_{001}$ is the difference of the reflectivity for normally incident light polarized along the $1\bar{1}0$ and 001 directions. The results for our bond model are shown in Fig. 3 along with the experimental data[49] and the results for a simple fcc lattice of isotropic dipoles.[50] We notice that the bond model has a good agreement with experiment, as good as that of the single-fcc model. We mention, though, that a similar model for SHG, with only one fcc lattice of isotropic polarizable entities,[34,33] each representing a tetrahedral arrangement of bonds, cannot reproduce either the bulk SHG anisotropy, which is evident in the experiments on the (001) surface,[5] or the resonant peak observed at 3.3 eV.[17]

Now we turn our attention to the nonlinear anisotropy. Following Refs. 13 and 14, we write for p-polarized SH output

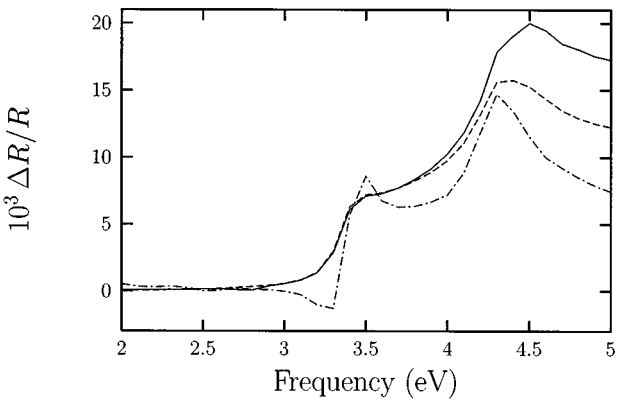

FIG. 3. Normal incidence anisotropy of the linear reflectance $\Delta R/R$ of a Si(110) surface as a function of frequency ω. We show results calculated with our bond model (solid line) and for a single fcc lattice of isotropic tetrahedral polarizable entities (dashed line) together with experimental results (dashed-dotted line).

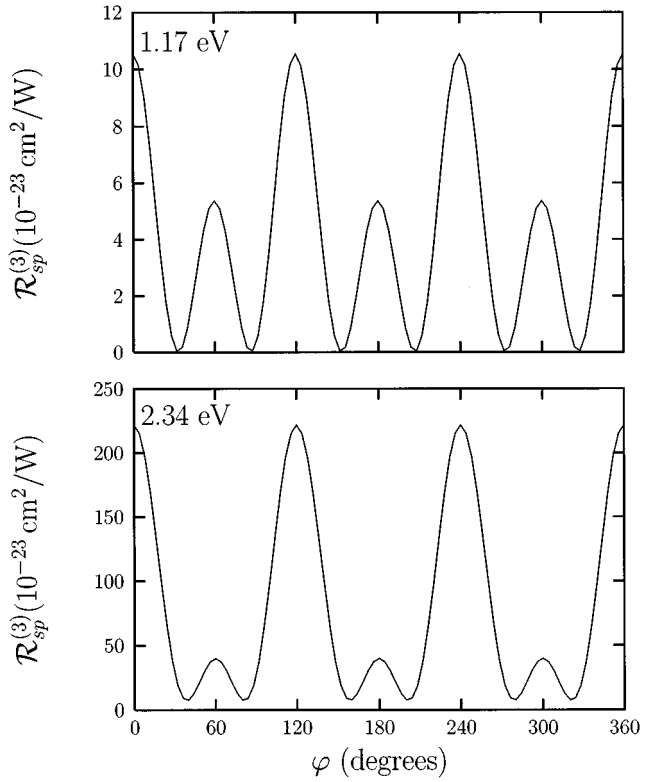

FIG. 4. s-in p-out SHG efficiency $\mathcal{R}_{sp}^{(3)}$ as a function of the azimuthal angle φ calculated for Si(111). The angle of incidence is $\theta = 45°$. The top (bottom) panel is for $\hbar\omega = 1.17$ eV ($\hbar\omega = 2.34$ eV).

$$\mathcal{R}_{ip}^{(m)}(\omega) = |a_i^{(m)}(\omega) + c_i^{(m)}(\omega)\cos(m\varphi)|^2, \tag{76}$$

and for s-polarized SH output

$$\mathcal{R}_{is}^{(m)}(\omega) = |b_i^{(m)}(\omega)\sin(m\varphi)|^2, \tag{77}$$

where i stands for the fundamental input polarization, which could be either s or p, m denotes the rotational symmetry of the surface, $m=3$ for the (111) face, whereas $m=4$ for the (001) face, and φ is the azimuthal angle. The complex functions $a(\omega)$, $b(\omega)$, and $c(\omega)$ depend on the macroscopic susceptibilities $\gamma(\omega)$, $\zeta(\omega)$, and $\vec{\chi}^{(s)}(\omega)$, as well as on the angle of incidence θ and bulk dielectric function $\epsilon(\omega)$ through Fresnel factors. These relationships can be found in Refs. 13 and 14. From them it follows that $c^{(4)}$ and $b^{(4)}$ depend only on ζ (besides the Fresnel factors), and therefore the azimuthal anisotropy of the (001) face originates in the bulk, regardless of the input-output polarizations. Also, for the (111) face we have that $\mathcal{R}_{ip}^{(3)}$ vs φ displays three peaks at $\varphi_n = 2n\pi/3$ with $n=0,1,2$ (i.e., threefold symmetry), and depending on the relative phase values between $a_i^{(3)}$ and $c_i^{(3)}$, there could be also three alternate peaks at $\varphi = \varphi_n \pm \pi/3$, for either s or p input polarization.

In Fig. 4 we plot $\mathcal{R}_{sp}^{(3)}$ vs φ for Si(111), with $\theta = 45°$. The top plot is for $\hbar\omega = 1.17$ eV and the bottom one is for $\hbar\omega = 2.34$ eV. The parameters $\omega_\perp$ and ω_p that describe the perpendicular linear polarizability $\alpha_\perp$ [Eq. (74)] were obtained by fitting these plots to the corresponding experiments given in Refs. 2 and 14. We see that there is an alternate

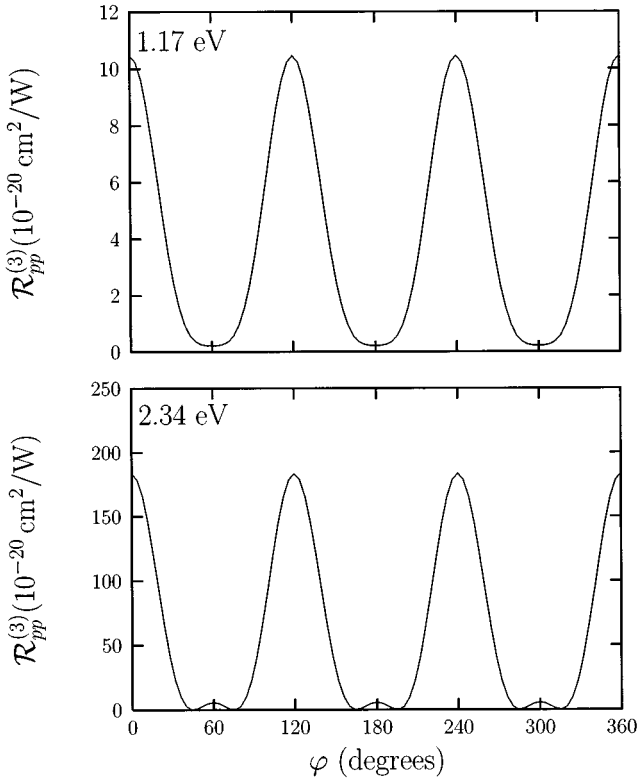

FIG. 5. p-in p-out SHG efficiency $\mathcal{R}^{(3)}_{pp}$ as a function of the azimuthal angle φ calculated for Si(111). The angle of incidence is $\theta=45°$. The top (bottom) panel is for $\hbar\omega=1.17$ eV ($\hbar\omega=2.34$ eV).

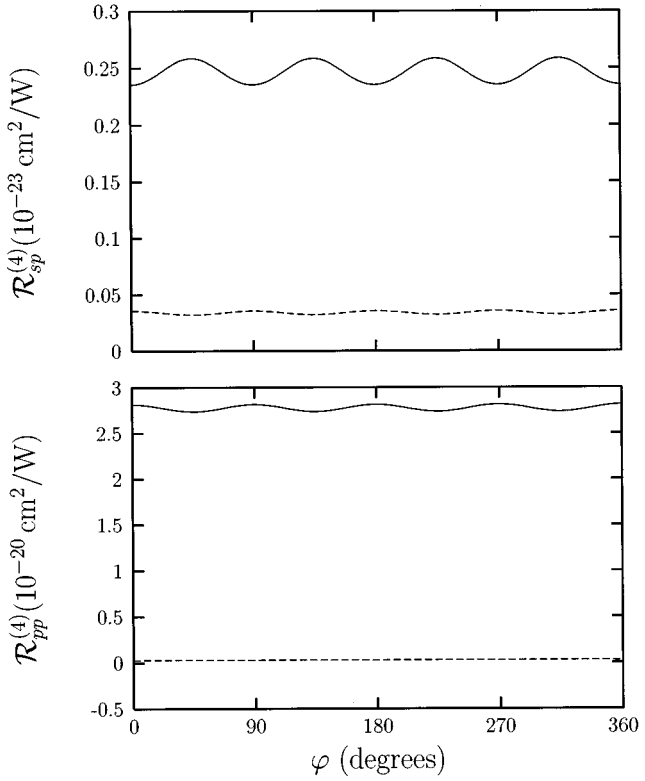

FIG. 6. SHG efficiency $\mathcal{R}^{(4)}$ as a function of the azimuthal angle φ for Si(001). The angle of incidence is $\theta=45°$, and we fixed $\hbar\omega=1.17$ eV (dashed line) and $\hbar\omega=2.34$ eV (solid line). The top (bottom) panel is for $s\rightarrow P$ ($p\rightarrow P$) polarization.

peak at $\varphi=60°,180°$, and $300°$, and that the ratio between these and the larger ones at $\varphi=0°,120°$, and $240°$ gets smaller for larger frequencies. On the other hand, Fig. 5 shows $\mathcal{R}^{(3)}_{pp}$ vs φ for Si(111), where $\theta=45°$ and for 1.17 eV and 2.34 eV. For 1.17 eV, we only see the peaks at $\varphi=0°,120°$, and $240°$ and the vanishing of the alternate peaks gives a minimum just like in the experimental results of Ref. 51. For 2.34 eV we get a very small alternate peak which was not detected experimentally.[5] However, its calculated height is smaller than the experimental resolution. Notice the change of scale by a factor of 1000 between Figs. 4 and 5. This big difference in signal strength arises from the different magnitude of the Fresnel factors for s and p incoming polarization.

In the top panel of Fig. 6 we display $\mathcal{R}^{(4)}_{sp}$ vs φ for Si(001), where $\theta=45°$ and for $\hbar\omega=1.17$ eV and 2.34 eV. We notice that ζ produces indeed a small anisotropy at 2.34 eV, which becomes even smaller at 1.17 eV, as is clearly shown in the experimental results of Ref. 2. However, we notice a π phase difference between the oscillations of $\mathcal{R}^{(4)}_{sp}$ we calculated at 2.34 eV and at 1.17 eV. This phase reversal has not been experimentally reported. This may be due to an ambiguity in the origin of the azimuthal angle. For example, in Ref. 2 it was chosen for convenience of display only. Therefore, we suggest that in future experiments the initial direction against which one measures φ should remain fixed throughout the whole set of frequencies. Similarly, the lower panel of Fig. 6 displays $\mathcal{R}^{(4)}_{pp}$. Again, there is a small anisotropy produced by the bulk term ζ at 2.34 eV, which now becomes negligible at 1.17 eV. The experimental results of Ref. 5 confirm the result for 2.34 eV, and to our knowledge there are no experiments for this combination of polarization at 1.17 eV.

Figure 7 shows $\mathcal{R}^{(3)}_{ps}$ and $\mathcal{R}^{(3)}_{ss}$ vs φ for Si(111), at 2.34 eV and 1.17 eV, respectively, for $\theta=45°$. Since both are for s-polarized SH beams, they display a sixfold peak degeneracy [Eq. (77)]. These two efficiencies only depend on ζ and $\chi^{(s)}_{|||||}$ a component which is unique to the (111) face. Once again, these results are in qualitative agreement with the experimental counterparts at 2.34 eV and 1.17 eV from Refs. 5 and 2, respectively. Notice again the change of scale between both panels.

The calculated results shown above imply that the present model gives an accurate qualitative description of the major features for the anisotropic nature SHG in Si at 1.17 and 2.34 eV. We have also checked that our results also agree with the anisotropy recently measured at $\hbar\omega=1.6$ eV.[52] Moreover, the model allows a variation of the fundamental frequency, thus generating spectroscopic results for SHG. They will be discussed in the following subsection.

B. Spectroscopy

In the preceding section we concentrated on the angular dependence of the SHG efficiency for a few fixed frequencies. Recently, the availability of intense tunable lasers has permitted spectroscopic studies of SHG. In this subsection we present calculations of several SHG spectra for different faces of Si and combinations of in and out polarizations.

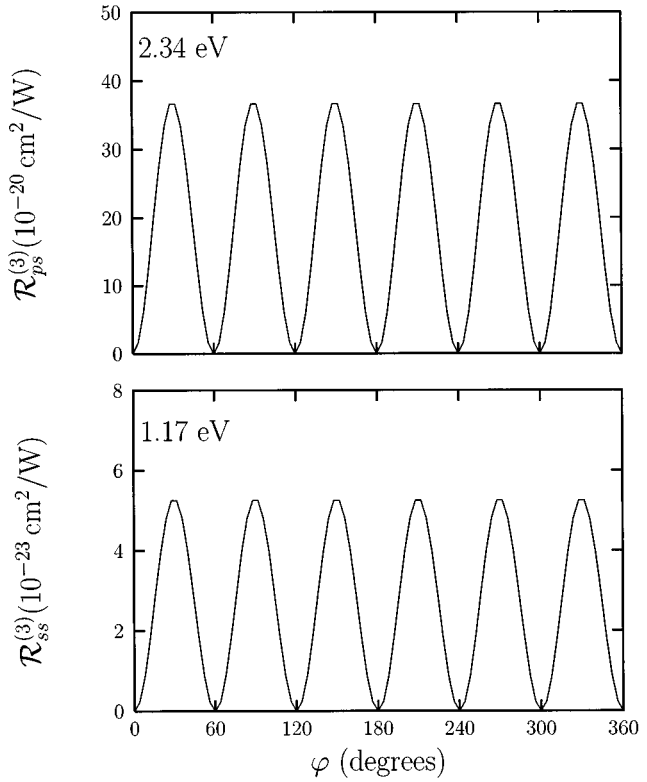

FIG. 7. SHG efficiency $\mathcal{R}^{(3)}$ as a function of the azimuthal angle φ for Si(111). The angle of incidence is $\theta=45°$. The top (bottom) panel is for $p\rightarrow S$ ($s\rightarrow S$) polarization and $\hbar\omega=2.34$ eV ($\hbar\omega=1.17$ eV).

Here we use the same parameters $\omega_\perp$ and ω_p as in the preceding subsection, with no further fitting. We constrain ourselves to a range that only goes up to 3 eV, since we expect spurious effects as the second-harmonic frequency gets close to the resonant frequency $\hbar\omega_\perp=7.17$ eV.

First, we present the values for the nonlinear susceptibilities as a function of frequency for Si(111). In Fig. 8, we show γ, ζ, and the four different independent components of $\vec{\chi}^{(s)}$. We notice that the surface susceptibilities $\chi^{(s)}_{\parallel\parallel\perp}$, $\chi^{(s)}_{\perp\parallel\parallel}$, and $\chi^{(s)}_{\parallel\parallel\parallel}$ have strong resonances at $\hbar\omega\approx1.75$ eV. For $\chi^{(s)}_{\perp\perp\perp}$ and the bulk components γ and ζ there is no structure and they are in general smaller than the other surface components, which are dominated by $\chi^{(s)}_{\parallel\parallel\parallel}$ In Fig. 9 we show the SHG efficiency spectra of Si(111) $\mathcal{R}^{(3)}_{sp}$ vs ω for $\theta=45°$, and for $\varphi=0°$ and 60°, which correspond to the large and small peaks of Fig. 4. We also plot the ratio between the height of these two lines. We clearly notice that there is a strong frequency dependence of both spectra. For instance, $\mathcal{R}^{(3)}_{sp}$ ($\varphi=60°$) has a maximum at 1.17 eV, and is practically null at 1.4 eV. These structures appear also in the quotient between both spectra, a feature that could be experimentally explored quantitatively, even without making absolute measurements. Even more dramatic is the large resonance for both orientations at $\approx$ 1.75 eV, whose position and width $\hbar\Delta\omega\approx0.14$ eV is in agreement with recent experiments.[17]

Indeed, SHG spectra have recently been measured for different clean, oxidized, and adsorbate covered surfaces of Si.[17–19] These spectra show a well developed peak close to $2\omega=3.3$ eV. Its position and its relative insensitivity to sur-

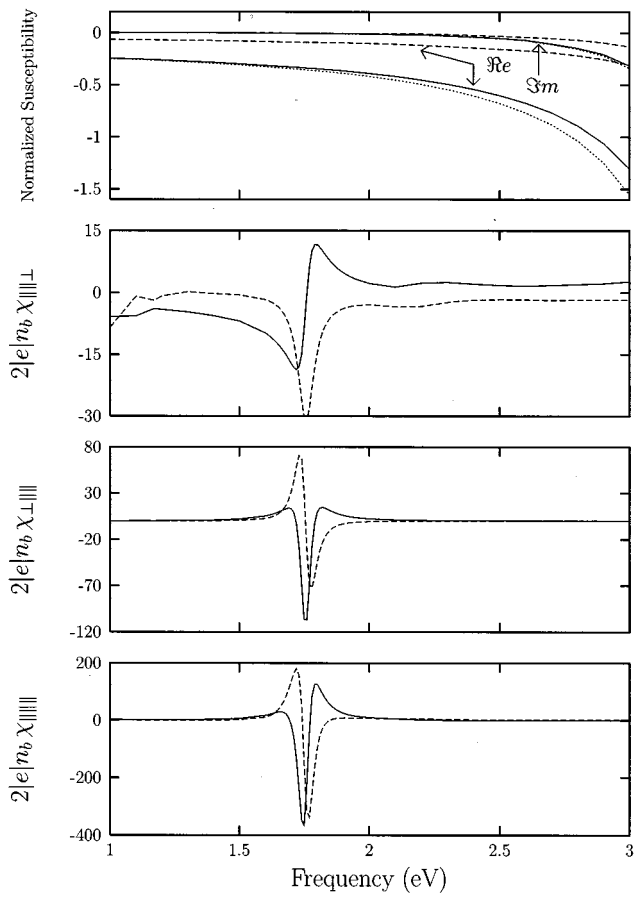

FIG. 8. Surface and bulk nonlinear susceptibilities as a function of frequency for Si(111). The first panel shows $2|e|n_b\gamma$ (dashed line), $2|e|n_b\zeta$ (dotted line), and $2|e|n_b\chi^{(s)}_{\perp\perp\perp}$ (solid line). In the other panels the corresponding component of $\vec{\chi}^{(s)}$ is indicated. Notice the resonant structure around 1.75 eV.

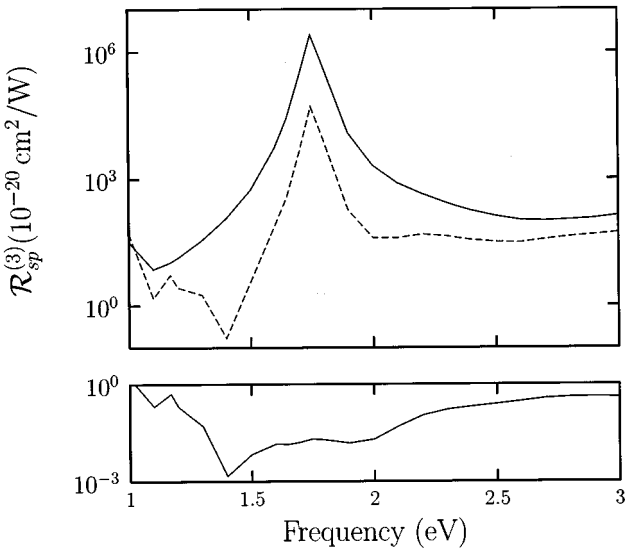

FIG. 9. SHG efficiency $\mathcal{R}^{(3)}_{sp}$ as a function of frequency for Si(111) (top panel). The angle of incidence is $\theta=45°$ and the azimuthal angles are $\varphi=0°$ (solid) and $\varphi=60°$ (dashed); they correspond to the peaks of Fig. 4. We also show the ratio of these two peaks in the bottom panel.

face conditions suggest that it is originated from a bulk transition between the valence and conduction bands which becomes SH electric-dipolarly active due to distortions in the crystalline structure close to the surface. To account for strain within the first few layers, we introduce a parameter $\Delta = d_1/d_B - 1$, where d_B is the separation between consecutive fcc planes in the bulk, and d_1 the corresponding separation between the first and second layers. For the ($\Delta = 0$) bulk-truncated (001) crystal we find a structureless spectrum, which is barely modified by stretching d_1. However, if we shrink d_1 by as little as 5% a very well developed peak appears[39] at $\hbar\omega = 1.65$ eV, with a width $\hbar\Delta\omega \approx 0.14$ eV in excellent agreement with experiment. These results can be appreciated in Fig. 1 of Ref. 39, which displays $\mathcal{R}^{(4)}_{pp}(\omega)$ calculated for light incident on Si(001) at an angle $\theta = 45°$ and $\varphi = 30°$. For even larger contractions, the height of the peak increases but its position remains mostly unchanged. Notice the huge change of scale between Fig. 1 of Ref. 39 and Fig. 9. The height of the latter is five orders of magnitude larger than that of the former. We have seen above that the (111) crystalline face presents a peak at 1.75 eV, as shown in Fig. 9, even when undistorted. While for the (111) face the peak comes from $\chi^{(s)}_{\parallel\parallel\perp}$, $\chi^{(s)}_{\perp\parallel\parallel}$, and $\chi^{(s)}_{\parallel\parallel\parallel}$ as can be appreciated from Fig. 8, for the (001) face the peak only comes from $\chi^{(s)}_{\parallel\parallel\perp}$, which is shown in Fig. 3 of Ref. 39.

Our results agree with the interpretation of the first experimental spectra[17,19] in that the origin of the resonance is surface originated. This was further confirmed through nonlinear electroreflectance spectroscopy (NER),[20,21] where it was found that this resonance does not depend on applied static electric fields, whereas a field dependent dipolar bulk transition was found nearby. The latter is missing in our results since in the absence of an applied static electric field two-photon dipolar transitions are symmetry-forbidden within the bulk. However, in Ref. 17 the peak at 3.3 eV was associated with a resonance in the normal component of the surface response $\chi^{(s)}_{\perp\perp\perp}$. This assignment was based on the angle-of-incidence dependence of the signal.[53] In Ref. 19 no resonance in the isotropic contribution to the efficiency of SHG from the (111) surface for $s \rightarrow p$ polarization $\mathcal{R}^{(3)}_{sp}$ was found. This indicates that $\chi^{(s)}_{\perp\parallel\parallel}$ does not resonate. This was taken as a further argument for the $\chi^{(s)}_{\perp\perp\perp}$ resonance,[19] although the possibility[21] of a resonance in $\chi^{(s)}_{\parallel\perp\parallel}$ seems not to have been contemplated.[19] Our results, shown in Fig. 8, display a resonance, although small, in $\chi^{(s)}_{\parallel\perp\parallel}$, a much larger resonance in $\chi^{(s)}_{\perp\parallel\parallel}$, and no resonance at all in $\chi^{(s)}_{\perp\perp\perp}$. The latter is also absent in Fig. 3 of Ref. 39. These theoretical results are contrary to the interpretation of experiment in Refs. 17 and 19. Since we only accounted for the surface local field effect in our theory, it is feasible to find a mechanism to provide the resonance we did not find in $\chi_{\perp\perp\perp}$. It seems more difficult to conceive a mechanism to eliminate the resonance we did find in $\chi_{\perp\parallel\parallel}$. However, there is still some disagreement on the identification of the tensor components responsible for the surface resonance[21] and panel (a) of Fig. 2 of Ref. 21 does show structure in the isotropic contribution to $\mathcal{R}^{(3)}_{sp}$, which necessarily comes from a resonance in $\chi^{(s)}_{\perp\parallel\parallel}$. Moreover, Pedersen and Morgen[54] have

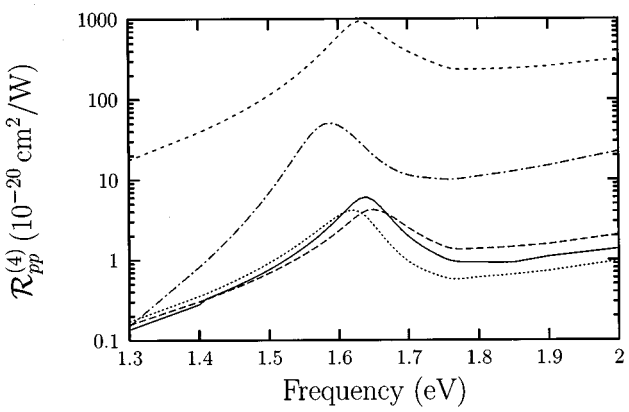

FIG. 10. SHG efficiency $\mathcal{R}^{(4)}_{pp}$ as a function of frequency for Si(001) and for a relaxation $\Delta = -0.05$. The angle of incidence is $\theta = 45°$, the azimuthal angle is $\phi = 30°$. For the solid line we took the surface polarizability $\vec{\alpha}_s(\omega)$ equal to the bulk polarizability $\vec{\alpha}_b(\omega)$, as in our previous figures. We also show results for the case when $\alpha_s(\omega) = 2\alpha_b(\omega)$ (dash-dotted) and when $\alpha_s(\omega) = 0.5\alpha_b(\omega)$ (short-dashed). Finally, we considered the case of a constant surface polarizability $\vec{\alpha}_s(\omega) = \vec{\alpha}_b(2.34\text{ eV})$ and $\vec{\alpha}_s(2\omega) = \vec{\alpha}_b(4.68\text{ eV})$ (dotted), and similarly $\vec{\alpha}_s(\omega) = \vec{\alpha}_b(1.17\text{ eV})$ and $\vec{\alpha}_s(2\omega) = \vec{\alpha}_b(2.34\text{ eV})$ (long dashed).

clearly observed very recently resonances in $\chi^{(s)}_{\perp\parallel\parallel}$ and in $\chi^{(s)}_{\parallel\parallel\parallel}$ at $2\omega = 3.4$ eV for Si (111)7×7, besides a resonance in $\chi^{(s)}_{\perp\perp\perp}$ at $2\omega = 3.3$ eV.

It has been found experimentally that the peaks close to $\hbar\omega = 1.65$ eV in the SHG spectra of both Si(001) and (111) surfaces are quite insensitive to the surface condition.[17] They appear on clean reconstructed samples and on samples oxidized under different conditions. The electronic structure of these systems is expected to be quite different at the surface, and so must be their polarizability. In our calculation we assumed the same polarizability at the surface and at the bulk, and we accounted only for the change in the local field and its spatial variation at the surface. In order to explore the robustness of the SHG resonant peak under surface perturbations, we have calculated the SHG efficiency spectra for Si(001) making arbitrary modifications to the polarizability of its first layer of bonds. Remarkably, the position of the resonant peak and its relative height over its baseline are not significantly changed by rather large changes to the surface polarizability. This is appreciated, for instance, in Fig. 10, where we show results obtained for the cases of surface polarizabilities that double and that halve the bulk polarizability. We also show results for constant surface polarizabilities that were fixed at the values of the bulk polarizabilities that were fitted to the SHG anisotropy at 1.17 and 2.34 eV. The reason for this lack of sensitivity in the resonance position is that the layer-by-layer polarization peaks at the subsurface bonds instead of at the topmost layer, as shown in Fig. 11.

V. CONCLUSIONS

In summary, we developed a model for the surface SHG of crystals with the structure of diamond which takes into account the nonlinear polarization induced by the microscopic spatial variation of the linear local field. Our model consists of four interpenetrated fcc lattices of anisotropic po-

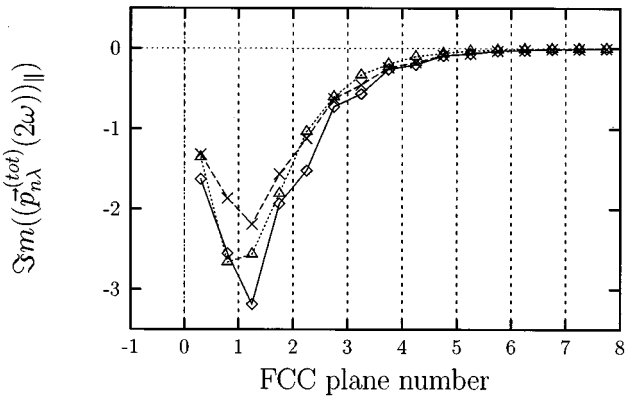

FIG. 11. Dipole moment $\mathrm{Im}((\vec{p}^{(\mathrm{tot})}_{n\lambda}(2\omega))_{\|})$ induced in the bond $n\lambda$ as a function of the position $z_{n\lambda}$ of its centroid (we summed over bonds with the same $z_{n\lambda}$). The rhombi correspond to the solid line in Fig. 10 and were calculated at the frequency of its peak. Similarly, the triangles (crosses) correspond to the dotted (long-dashed) line of Fig. 10.

larizable bonds, each of which responds nonlinearly to the inhomogeneous local field with a microscopic hyperpolarizability that we wrote in terms of the linear polarizability. The latter was obtained from the bulk dielectric function, the geometry of the crystal, and two parameters describing the response of an individual bond in the direction normal to its axis, which were fitted to a few SHG anisotropy measurements on the (001) and (111) surface. Our model yields a linear reflectance difference spectra for the (110) surface in agreement with experiment. We remark that a similar model with only one fcc lattice of isotropic polarizable entities,[34,33] each representing a tetrahedral arrangement of bonds, cannot reproduce either the bulk SHG anisotropy, which is evident in the experiments on the (001) surface,[5] or the peak at $2\hbar\omega = 3.3$ eV. Although we have neglected all effects due to the surface modification of the electronic structure, we have obtained agreement with the first experimental spectra available for different surfaces of Si. For a bulk truncated (001) face we obtained a structureless spectrum which acquired a well defined peak when we allowed for surface relaxation. For the (111) face a much larger peak at a nearby frequency was found even without relaxation. In our calculation, the position of the peak differs from that of the bulk interband transitions due to a local field induced shift. Our results also suggest a possible explanation for the lack of sensitivity of the SHG spectra on the surface treatment, since they show that the total SH polarization peaks below the first crystalline plane, and it extends for a few other planes before vanishing into the bulk. We have recalculated the SHG spectra employing different microscopic surface polarizabilities and have found that the peak's position is very robust.[39] A very large change, such as that expected for a hydrogenated surface, would be necessary to remove it.[17]

In conclusion, our results yield a plausible explanation for the experimentally found SHG resonance. The peak in our model does not arise from a SH transition that becomes dipolarly allowed due to a lattice distortion.[17] Rather, it comes from the large uncompensated local field gradient at the surface and is therefore allowed even for a centrosymmetrical bond, but in the noncentrosymmetrical environment of the surface. According to our model, the peak observed on the (111) surface is present even without surface relaxation, so its observation should not be interpreted as evidence for a lattice expansion. On the other hand, the peak on the (001) surface only arises within our model in the presence of a surface contraction. In this paper we have restricted our attention to the surface local field effect, and further theoretical developments would be necessary to find the contributions to SHG from other effects. Theoretical work along this line is required to understand and eliminate the apparent discrepancies between our theory and some consequences of experiment, such as the identification of the susceptibility components responsible for the observed resonances. Also, further experimental work would be welcome to fully disentangle the role of the different susceptibility components.

ACKNOWLEDGMENTS

This research was partially supported by CONACyT-3246-E9308 (B.M.S.) and by DGAPA-UNAM-IN102493 and IN104594 (W.L.M.). Also, B.M.S. would like to acknowledge enlightening discussions with V. Arroyo.

[1] Bernardo S. Mendoza and W. Luis Mochán, Phys. Rev. B **53**, 4999 (1996).

[2] J. A. Litwin, J. E. Sipe, and H. M. van Driel, Phys. Rev. B **31**, 5543 (1985). Notice that in this reference the panels (a) and (b) of Fig. 3 are interchanged, as pointed out in Ref. 20 of Sipe *et al.* (Ref. 14).

[3] D. Guidotti, T. A. Driscoll, and H. J. Gerristen, Solid State Commun. **46**, 337 (1983).

[4] T. A. Driscoll and D. Guidotti, Phys. Rev. B **28**, 1171 (1983).

[5] H. W. K. Tom, T. F. Heinz, and Y. R. Shen, Phys. Rev. Lett. **51**, 1983 (1983).

[6] M. A. Varheijen, C. W. van Hasselt, and Th. Rasing, Surf. Sci. **251/252**, 467 (1991).

[7] C. W. van Hasselt, M. A. Verheijen, and Th. Rasing, Phys. Rev. B **42**, 9263 (1990).

[8] C. Jordan, E. J. Canto-Said, and G. Markowsky, Appl. Phys. B **58**, 111 (1994).

[9] R. W. J. Hollering and M. Barmentlo, Opt. Commun. **88**, 141 (1992).

[10] S. V. Govorkov *et al.*, Appl. Phys. A **50**, 439 (1990).

[11] S. V. Govorkov *et al.*, J. Opt. Soc. Am. B **6**, 1117 (1989).

[12] L. L. Kulyuk *et al.*, J. Opt. Soc. Am. B **8**, 1766 (1991).

[13] O. A. Aktsipetrov, I. M. Baranova, and Yu. A.Il'inskii, Zh. Éksp. Teor. Fiz. **91**, 287 (1986) [Sov. Phys. JETP **64**, 167 (1986)].

[14] J. E. Sipe, D. J. Moss, and H. M. van Driel, Phys. Rev. B **35**, 1129 (1987).

[15] G. Lüpke, D. J. Bottomley, and H. M. van Driel, Phys. Rev. B **47**, 10 389 (1993).

[16] G. Lüpke, D. J. Bottomley, and H. M. van Driel, J. Opt. Soc. Am. B **11**, 33 (1994).

[17] W. Daum *et al.*, Phys. Rev. Lett. **71**, 1234 (1993).
[18] J. F. McGilp *et al.*, Opt. Eng. **33**, 3895 (1994).
[19] C. Meyer *et al.*, Phys. Rev. Lett. **74**, 3001 (1995).
[20] J. I. Dadap, *et al.*, Phys. Rev. B **53**, R7607 (1996).
[21] P. Godefroy *et al.*, Appl. Phys. Lett. **68**, 1981 (1996).
[22] J. E. Sipe, V. C. Y. So, M. Fukui, and G. I. Stegeman, Phys. Rev. B **21**, 4389 (1980).
[23] J. E. Sipe and G. I. Stegeman, in *Surface Polaritons*, edited by V. M. Agranovich and D. L. Mills (North Holland, Amsterdam, 1982).
[24] M. Corvi and W. L. Schaich, Phys. Rev. B **33**, 3688 (1986).
[25] W. L. Schaich and A. Liebsch, Phys. Rev. B **37**, 6187 (1988).
[26] M. Weber and A. Liebsch, Phys. Rev. B **35**, 7411 (1987).
[27] A. Liebsch, Phys. Rev. Lett. **61**, 1233 (1988); **61**, 1897(E) (1988).
[28] A. Liebsch and W. L. Schaich, Phys. Rev. B **40**, 5401 (1989).
[29] J. A. Maytorena, W. Luis Mochán, and Bernardo S. Mendoza, Phys. Rev B **51**, 2556 (1995).
[30] A. V. Petukhov, Phys. Rev. B **42**, 9387 (1990); A. V. Petukhov and A. Liebsch, Surf. Sci. **294**, 381 (1993).
[31] Jesús Tarriba and W. Luis Mochán, Phys. Rev. B **46**, 12 909 (1992); Yves Borensztein, W. Luis Mochán, Jesús Tarriba, Rubén G. Barrera, and A. Tadjeddine, Phys. Rev. Lett. **71**, 2334 (1993).
[32] W. L. Mochán and B. S. Mendoza, J. Phys. Condens. Matter **33**, A183 (1993).
[33] W. L. Schaich and B. S. Mendoza, Phys. Rev. B **45**, 14 279 (1992).
[34] B. S. Mendoza, J. Phys. Condens. Matter **5**, A181 (1993).
[35] C. M. J. Wijers, Th. Rasing, and R. W. J. Hollering, Solid State Commun. **85**, 233 (1993); C. M. J. Wijers, P. L. de Boeij, C. W. van Hasselt, and Th. Rasing, *ibid.* **93**, 17 (1995).
[36] M. Cini, R. del Sole, and L. Reining, Surf. Sci. **287-288**, 693 (1993); L. Reining, R. del Sole, M. Cini, and J. G. Ping, Phys. Rev. B **50**, 8411 (1994).
[37] W. L. Mochán and R. G. Barrera, Phys. Rev. Lett. **55**, 1192 (1985); **56**, 2221 (1986).
[38] C. H. Patterson, D. Wearie, and J. F. McGilp, J. Phys. Condens. Matter **4,** 4017 (1992).
[39] Bernardo S. Mendoza and W. Luis Mochán, Phys. Rev. B **53**, R10 473 (1996).
[40] R. Kubo, J. Phys. Soc. Jpn. **12**, 570 (1957).
[41] F. W. de Wette and G. E. Schacher, Phys. Rev. **137**, A78 (1965).
[42] W. Luis Mochán and Rubén G. Barrera, Phys. Rev. B **32**, 4984 (1985).
[43] J. D. Jackson, *Classical Electrodynamics* (Wiley, New York, 1975), Sec. 6.7.
[44] P. Guyot-Sionnest and Y. R. Shen, Phys. Rev. B **35**, 4420 (1987).
[45] P. Guyot-Sionnest and Y. R. Shen, Phys. Rev. B **38**, 7985 (1988).
[46] E. Palik, *Handbook of Optical Constants of Solids* (Academic Press, New York, 1991), Vol. 1; D. E. Aspnes and A. A. Studna, Phys. Rev. B **27**, 985 (1983).
[47] Charlotte E. Moore, *Atomic Energy Levels* (NBS, Washington, 1970), p. 144.
[48] W. Hanke and L. J. Sham, Phys. Rev. B **21**, 4656 (1980); E. Fiorino and R. del Sole, Phys. Status Solidi B **119**, 315 (1983).
[49] D. E. Aspnes and A. A. Studna, Phys. Rev. Lett. **54**, 1956 (1985).
[50] R. Del Sole, W. L. Mochán, and R. G. Barrera, Phys. Rev. B **43**, 2136 (1991).
[51] T. A. Driscoll and D. Guidotti, Phys. Rev. B **28**, 1171 (1983).
[52] T. Y. F. Tsang, Bull. Am. Phys. Soc. **40**, 511 (1995); Phys. Rev. A **52**, 4116 (1995).
[53] W. Daum *et al.*, Phys. Scr. **T49**, 513 (1993).
[54] K. Pedersen and P. Morgen, Surf. Sci. (to be published).